

Anderson impurity model in nonequilibrium: analytical results versus quantum Monte Carlo data

L. Mühlbacher,¹ D. F. Urban,¹ and A. Komnik²

¹*Physikalisches Institut, Albert-Ludwigs-Universität Freiburg,
Hermann-Herder-Str. 3, D-79104 Freiburg, Germany*

²*Institut für Theoretische Physik, Ruprecht-Karls-Universität Heidelberg,
Philosophenweg 19, D-69120 Heidelberg, Germany*

(Dated: February 10, 2011)

We analyze the spectral function of the single-impurity two-terminal Anderson model at finite voltage using the recently developed diagrammatic quantum Monte Carlo technique as well as perturbation theory. In the (particle-hole-)symmetric case we find an excellent agreement of the numerical data with the perturbative results of second order up to interaction strengths $U/\Gamma \approx 2$, where Γ is the transparency of the impurity-electrode interface. The analytical results are obtained in form of the nonequilibrium self-energy for which we present explicit formulas in the closed form at arbitrary bias voltage. We observe an increase of the spectral density around zero energy brought about by the Kondo effect. Our analysis suggests that a finite applied voltage V acts as an effective temperature of the system. We conclude that at voltages significantly larger than the equilibrium Kondo temperature there is a complete suppression of the Kondo effect and no resonance splitting can be observed. We confirm this scenario by comparison of the numerical data with the perturbative results.

PACS numbers: 73.63.Kv, 75.20.Hr, 73.23.-b

I. INTRODUCTION

Despite its simplicity the Anderson impurity model (AIM)¹ contains a surprising amount of interesting physics. Under equilibrium conditions, when the singly occupied dot level lies deep below the chemical potential of the fermion continuum and when the Coulomb repulsion U prohibits double occupation of the dot, the impurity spectral function, i.e. the impurity density of states (DOS), is known to develop a sharp Kondo (aka Abrikosov-Suhl) resonance which is located at the chemical potential of the fermion continuum. It is observable at relatively low temperatures $T < T_K$, where the Kondo temperature T_K is an estimate for the resonance width. This is the essence of the conventional Kondo effect.^{2,3}

In recent years a quite natural extension of Anderson's original idea, namely a setup in which the impurity is coupled to two fermion continua, came to attention as its experimental realization became feasible.⁴⁻⁶ A particularly interesting direction of research is the investigation of the nonequilibrium transport as well as of the Kondo effect which has been quite successfully approached analytically, see e. g. Refs. [7–16], as well as numerically, see e. g. Refs. [17–22]. Yet another but related research direction is concerned with the nonequilibrium transport in a pure Kondo model, see e. g. Refs. [23–27].

In order to induce a finite electric current through a quantum dot at least two electrodes with *different* chemical potentials are necessary. Contrary to the naive expectation that coupling to two fermionic continua may lead to a two-channel Kondo effect the original resonance was predicted to split into two peaks which are positioned at the two chemical potentials.^{8,24,25,28,29} Electron transport between the leads is accompanied by spin-flip pro-

cesses which essentially break the symmetry necessary to drive the system into the two-channel Kondo fixed point. On the other hand, exactly those spin-flip processes participate in the RG flow and grow stronger toward low energies thereby being responsible for almost perfect effective electron transmission (at the Fermi edge in equilibrium) across the impurity far below T_K . In the case of a finite applied voltage V there is a constant spin-flip rate associated with the current flowing through the system, so that the Kondo peaks are weaker and broadened in comparison to the equilibrium situation.^{8,30} This splitting as well as the broadening of the Kondo peaks are difficult to access in the two-terminal setup. Therefore a three-terminal approach for the spectral function measurement has been put forward,^{31,32} which shortly afterwards was implemented experimentally.^{33,34}

Although by now a number of studies of multi-terminal Kondo/Anderson setups have been conducted, see e. g. Refs. [35,36], it is desirable to analyze the problem with non-approximative methods in order to cover the full Kondo crossover.¹⁷ The recently developed diagrammatic quantum Monte Carlo (diagMC) approach not only allows to simulate finite voltage transport but also reliably works even at zero temperature.³⁷⁻⁴¹ In this paper the diagMC is applied in order to calculate the impurity spectral function of the AIM under nonequilibrium conditions with special emphasis on the Kondo effect related features. The numerical data is then compared with the results of the analytical perturbative expansion in interaction strength U . We find that as soon as the bias voltage exceeds the equilibrium T_K the Kondo effect related features in the spectral function rapidly deteriorate. By comparison of the numerical data with the perturbative results we conclude that the large finite voltage has sim-

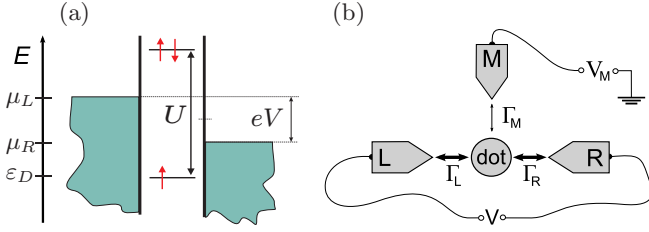


FIG. 1: (a) Level structure of the quantum dot with respect to the two fermion continua (leads) at chemical potentials $\mu_{L/R}$. The dot level ϵ_D corresponding to single occupation lies below $\mu_{L/R}$ while the energy level for double occupation $\epsilon_D + U > \mu_{L/R}$ is augmented by U due to Coulomb repulsion. (b) Sketch of the setup. For the analytical analysis we consider the two terminal setup in which the quantum dot is coupled to a left (L) and right (R) lead via electron tunneling $\propto \Gamma_{L/R} \equiv \Gamma$. For the numerical analysis it is advantageous to add a third measuring electrode M which is only very weakly coupled to the quantum dot and to consider the limit $\Gamma_M \rightarrow 0$.

ilar consequences as finite temperature. This explains why the Kondo features are so weak and the resonance doubling is not observable at all.

The outline of the paper is as follows: In Sec. II we formulate the problem and identify the most interesting energy regimes. The perturbative results for the self-energy and impurity DOS, for which we obtain analytical expressions in a closed form, are presented. Section III is devoted to the details of the numerical implementation of the diagMC scheme. Results are presented in Section IV, where the numerical data are compared with the perturbative result and the physical picture is discussed.

II. FORMULATION OF THE PROBLEM AND PERTURBATIVE RESULTS

We model the system in the canonical way using the Hamiltonian

$$H = H_0 + H_I + H_T. \quad (1)$$

Here H_0 contains both the uncoupled impurity level at energy ϵ_D which can be subject to a (local) magnetic field h , as well as the left/right contacting leads. The latter are assumed to be noninteracting fermion continua with field operators $\psi_{\alpha,\sigma}$, $\alpha = L/R$, kept at chemical potentials $\mu_{L/R}$. Here σ is the spin index.

$$H_0 = \sum_{\alpha,\sigma} H_{\alpha}[\psi_{\alpha,\sigma}] + \sum_{\sigma} (\epsilon_D + \mu_B g \sigma h/2) d_{\sigma}^{\dagger} d_{\sigma}, \quad (2)$$

where d_{σ} and d_{σ}^{\dagger} are the annihilation/creation operators of an electron on the impurity level. As usual, μ_B is Bohr's magneton and g is the Landé factor. Electron exchange between the electrodes and the impurity takes

place locally at $x = 0$ and is accomplished by

$$H_T = \gamma \sum_{\alpha,\sigma} d_{\sigma}^{\dagger} \psi_{\alpha,\sigma}(0) + \text{H.c.}, \quad (3)$$

where γ is the tunneling amplitude between dot level and electrode, which we for simplicity assume to be equal for both contacts.⁶⁶ Finally, Coulomb repulsion on the impurity is taken into account via the last term,

$$H_I = U n_{\uparrow} n_{\downarrow}, \quad (4)$$

where $n_{\sigma} = d_{\sigma}^{\dagger} d_{\sigma}$. Perhaps the most interesting parameter regime is the particle-hole symmetric one, when $h = 0$ and $\epsilon_D = -U/2$ (aka *symmetric* Anderson model), for which the level structure of the quantum dot is depicted in Fig. 1(a). Under equilibrium conditions this model is solvable by the Bethe Ansatz.^{3,42} This method works perfectly as far as thermodynamic properties are concerned but the extraction of single particle quantities, although in principle possible, still remains an open issue. The most important single particle quantity is the local impurity DOS (spectral function) $\rho_d(\omega)$. It is related to the Fourier transform of the retarded Green's function (GF) of the dot $D^R(\omega)$ via

$$\rho_d(\omega) = -2\text{Im} D^R(\omega), \quad (5)$$

where

$$D^R(t) = -i\Theta(t)\langle\{d_{\sigma}(t), d_{\sigma}^{\dagger}(0)\}\rangle. \quad (6)$$

Here $\{.,.\}$ denotes the anticommutator and $\Theta(t)$ is the Heavyside step function. In the interacting case, $D^R(\omega)$ can be expressed in terms of the self-energy $\Sigma^R(\omega)$,

$$D^R(\omega) = \frac{1}{\omega - i\Gamma - \Sigma^R(\omega)}. \quad (7)$$

Here $\Gamma = 2\pi\rho_0|\gamma|^2$ is the lead-dot contact transparency that depends on the tunneling amplitude γ and on the local DOS in the electrodes ρ_0 , which we assume to be only weakly energy-dependent. For simplicity of notation, we will use units for which $\Gamma \equiv 1$ in the following, so that Γ is the unit of energy.

As has been pointed out in Ref. [43] the spectral function plays an important role especially in nonequilibrium transport and the current through the dot is given by the Meir-Wingreen formula⁴³

$$I(V) = G_0 \int d\omega \rho_d(\omega) [n_L(\omega) - n_R(\omega)], \quad (8)$$

where $G_0 = 2e^2/h$ is the conductance quantum and $n_{L,R}(\omega) = [\exp((\omega - \mu_{L,R})/T) + 1]^{-1}$ are the Fermi distribution functions in the respective electrodes. First calculations of the spectral function use perturbation theory in U .⁴⁴⁻⁴⁹ The corresponding series turns out to be well-controlled and rapidly converging. Often there is no necessity for having the complete energy dependence

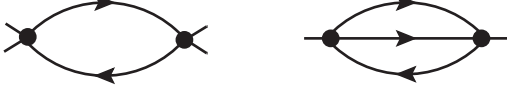


FIG. 2: Feynman diagrams for the polarization loop (left), and for the self-energy at second order, $\propto U^2$ (right).

of the spectral function (via e.g. the corresponding self-energies) at hand so that an expansion of $\rho_d(\omega)$ for low energies is sufficient. In all other situations there exist numerous studies also in nonequilibrium.^{7,10,37–41,50–53} However, analytical expressions in a closed form for the self-energy from the second order onwards do not yet exist.

For technical reasons the calculation of the self-energies has a number of advantages. Starting point are the impurity GF without interactions. With $H_I \equiv 0$ the Hamiltonian (1) is quadratic and can be trivially diagonalized even in nonequilibrium.⁵⁴ The noninteracting GF (we concentrate on the electron-hole symmetric case) read^{55,56}

$$\begin{aligned} D^{R,A}(\omega) &= \frac{1}{\omega \pm i}, \\ D^K(\omega) &= \frac{2i(n_L(\omega) + n_R(\omega) - 1)}{\omega^2 + 1}. \end{aligned} \quad (9)$$

Just as well we can work with the Keldysh GF $D^{kl}(\omega)$ which are related to the GFs in the RAK representation (9) by a simple rotation in Keldysh space.⁵⁷ As usual, the Keldysh indices $k, l = \pm$ denote the branch of the contour on which the final and initial times of the corresponding GF in the time domain are taken: $-$ for the time-ordered

one and $+$ for the anti-time-ordered one.

The lowest order self-energy, c.f. Fig. 2, contains two energy integrations and is given by

$$\begin{aligned} \Sigma^{kl}(\omega) &= - \int \frac{d\Omega d\epsilon}{(2\pi)^2} D^{kl}(\omega - \Omega) D^{lk}(\epsilon) D^{kl}(\epsilon + \Omega) \\ &= i \int \frac{d\epsilon}{2\pi} D^{kl}(\omega + \epsilon) \Pi^{lk}(\epsilon), \end{aligned} \quad (10)$$

where

$$\Pi^{lk}(\omega) = i \int \frac{d\epsilon}{2\pi} D^{lk}(\omega + \epsilon) D^{kl}(\epsilon) \quad (11)$$

is the generalized (Keldysh) polarization loop.⁶⁷ An explicit calculation of these quantities is tedious but straightforward. In the following we give the results only. The retarded polarization loop is given by⁵⁶

$$\Pi^R(\omega) = \Pi^{--}(\omega) - \Pi^{-+}(\omega) \quad (12)$$

$$= -\frac{1}{\pi} \frac{1}{\omega^2 + 2i\omega} \ln \left[\frac{(1 - i\omega)^2 + (V/2)^2}{1 + (V/2)^2} \right] \quad (13)$$

and we find the time-ordered polarisation loop to read

$$\begin{aligned} \Pi^{--}(\omega) &= \Pi^R(|\omega|) \\ &+ \frac{i}{\pi} \text{Im} \left[\frac{1}{\omega^2 + 2i|\omega|} \ln \left(\frac{|\omega| - V/2 + i}{V/2 + i} \right) \right] \Theta(|V| - |\omega|). \end{aligned} \quad (14)$$

The remaining Keldysh components can be inferred from relation (12) and the symmetry properties of Π^{kl} , namely $\Pi^{+-}(\omega) = \Pi^{-+}(-\omega)$ and $\Pi^{++}(\omega) = -\Pi^{--}(\omega)^*$. With these expressions at hand we perform the integral (10) and find the retarded self-energy to be given by

$$\begin{aligned} \Sigma^R(\omega) &= -\frac{3i}{(2\pi)^2} \left\{ \frac{1}{1 + \omega^2} \left[\frac{\pi^2 \omega}{3i} + \frac{1}{2} \ln^2 \left(\frac{i - V/2}{i + V/2} \right) + \sum_{\alpha, \beta = \pm} \text{Li}_2 \left(\beta \frac{\alpha V/2 - \omega}{\alpha V/2 + \beta i} \right) \right] \right. \\ &\quad \left. + \frac{1}{(i + \omega)(3i + \omega)} \left[\pi^2 - \frac{1}{2} \ln^2 \left(\frac{i - V/2}{i + V/2} \right) - \sum_{\alpha, \beta = \pm} \Lambda \left(\frac{2i + \omega - \alpha \beta V/2}{i + \alpha V/2} \right) \right] \right\}. \end{aligned} \quad (15)$$

Here Li_2 denotes the dilogarithm function and we have introduced

$$\Lambda(z) = \text{Li}_2(z) - i\pi \text{sgn}[\text{Im}(z)] \ln(z). \quad (16)$$

In equilibrium this expression simplifies considerably,

$$\begin{aligned} \Sigma_{eq}^R(\omega) &= -\frac{1}{\pi^2(1 + \omega^2)} \left(\frac{\pi^2}{4} \omega + 3i \text{Li}_2(i\omega) \right) \\ &+ \frac{3i}{\pi^2(i + \omega)(3i + \omega)} \left[\Lambda(2 - i\omega) - \frac{\pi^2}{4} \right]. \end{aligned} \quad (17)$$

Finally, the spectral function is given via Eqs. (5, 7). Its behavior as function of energy is depicted in Fig. 5 and discussed in section IV.

III. DIAGRAMMATIC MONTE CARLO SIMULATION METHOD

The recently developed refinements of the diagMC technique allow to access regimes of arbitrary interac-

tion strength and therefore make diagMC simulations a suitable tool for numerically investigating the AIM with large onsite Coulomb repulsion⁴¹. Moreover, this approach gives access to the transient behavior of the system after sudden switching of the tunneling coupling and therefore contributes to the rapidly developing research area investigating interaction quenches in quantum dots, see e.g. Refs. [27,58–63]. An advantage of diagMC is the possibility to explicitly implement the band structure of the electrodes. In this regard it can be seen as an ideal tool for discussing experimental results.

In principle, the dot spectral density can be measured using its immediate definition (5). However, as suggested in Refs. [31,32], the spectral function can more efficiently be deduced by adding an additional third probe electrode, which is only weakly coupled to the quantum dot, c.f. Fig. 1(b). The conductance of this ‘measuring’ electrode (denoted by the subscript ‘M’ in our notation) is given by

$$g_M(t) = \frac{d}{d\mu_M} I_M(t), \quad (18)$$

where I_M and μ_M are the current and chemical potential for the third contact, respectively. In the limit of vanishing coupling Γ_M , the spectral density is related to the steady state value ($t \rightarrow \infty$) of the conductance by^{31,32}

$$\rho_d(\mu_M) = \lim_{\Gamma_M \rightarrow 0} \Gamma_M^{-1} \lim_{t \rightarrow \infty} g_M(t). \quad (19)$$

An advantage of this approach is that it corresponds to the method used in experimental studies.³⁴

Following the lines of Refs. [37,39,52] the current through the contact α , with $\alpha \in \{L, M, R\}$, in the absence of magnetic fields is given by

$$I_{\alpha\sigma}(t) = -4\text{Im} \sum_{k \in L} \gamma_{\sigma k}(t) \text{tr} \left\{ W_0 a_{\alpha\sigma k}^\dagger(t) d_\sigma(t) \right\}, \quad (20)$$

where $a_{\alpha\sigma k}^\dagger$ is the momentum- k component of the $\psi_{\alpha\sigma}^\dagger(x)$ field operator and W_0 denotes the full initial density operator of the system (which we assume to factorize, with the dot being initially empty). Note that the tunneling amplitude $\gamma_{\alpha k}$ in Eq. (20) is explicitly energy/momentum dependent. This is necessary because contrary to the analytical calculations of the previous section, where an infinite flat band significantly simplifies the calculations, the use of a band with a finite width is essential in numerical approaches for exactly the same reason. An additional speed-up of the diagMC simulations is achieved by a smooth switch-on procedure accomplished by a time dependent coupling

$$\gamma_{\alpha k}(t) = g_\alpha(t) \gamma_{\alpha k}, \quad (21)$$

where $g_\alpha(t)$ interpolates smoothly between 0 at $t = 0$ and 1 within the switching time τ_{sw} .⁵² ($g_\alpha(t) = \sin^2[\pi t/(2\tau_{\text{sw}})]$ for $t < \tau_{\text{sw}}$ and $g_\alpha(t) = 1$ for $t \geq \tau_{\text{sw}}$) In the limit of a

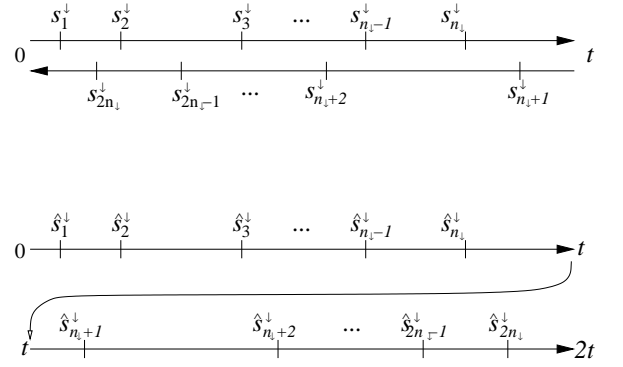


FIG. 3: Contour-ordered (top) and time-ordered (bottom) sequences of tunneling times.

quasi-continuous distribution of electronic energies in the leads, the time-dependent contact transparency reads

$$\Gamma_\alpha(\epsilon, t) = 2\pi\rho_\alpha(\epsilon)|\gamma_{\alpha k}(t)|^2 \equiv g_\alpha^2(t)\Gamma_\alpha(\epsilon), \quad (22)$$

where $\rho_\alpha(\epsilon)$ is the DOS of the leads.⁶⁴ For the numerical implementation we choose a flat band with the width $2\epsilon_c$ and temperature-smoothed boundaries.³⁷ The corresponding profile of $\Gamma_\alpha(\epsilon)$ is given by

$$\Gamma_\alpha(\epsilon) = \frac{\Gamma_\alpha}{[1 + e^{\beta(\epsilon - \epsilon_c)}][1 + e^{-\beta(\epsilon + \epsilon_c)}]}. \quad (23)$$

Time-dependent transport properties can be calculated by a diagMC scheme using the conventional breakdown of the time evolution operator. Since the corresponding formalism has been described in detail before,^{39,52} we restrict ourselves in the following to presenting the extensions of the formalism, i.e. the inclusion of the probe electrode.

Expanding the time evolution operator in terms of the dot-lead coupling yields a Dyson series where the integration variables corresponds to the times at which tunneling between the dot and the lead occurs. The contour-ordered kink sequence of the $2\tilde{n}_\sigma$ tunneling times s_j^σ of spin- σ charges is denoted by

$$\vec{s}^\sigma \equiv \{s_1^\sigma, s_2^\sigma, \dots, s_{2\tilde{n}_\sigma}^\sigma\}. \quad (24)$$

They reside on the closed real-time contour $s : 0 \rightarrow t \rightarrow 0$ (c.f. Fig. 3). The corresponding time ordered analogon is denoted by

$$\hat{s}_\sigma^\sigma \equiv \{\hat{s}_1^\sigma, \hat{s}_2^\sigma, \dots, \hat{s}_{2\tilde{n}_\sigma}^\sigma\}, \quad (25)$$

with

$$\hat{s}_j^\sigma = \begin{cases} s_j^\sigma & \text{for } j \leq n_\sigma, \\ 2t - s_j^\sigma & \text{for } j > n_\sigma, \end{cases} \quad (26)$$

where n_σ counts the number of spin- σ tunneling times on the forward time axis. Equation (20) can then be

conveniently expressed as

$$I_\alpha(t) = -2e \sum_{\substack{\tilde{n}_\uparrow=1 \\ \tilde{n}_\downarrow=0}}^{\infty} (-1)^{\tilde{n}_\uparrow+\tilde{n}_\downarrow} \int_0^{2t} d\hat{s}_\uparrow \int_0^{2t} d\hat{s}_\downarrow \\ \times \text{Re} \left\{ \mathcal{L}_\uparrow^{(\alpha)}(\hat{s}_\uparrow) \mathcal{L}_\downarrow(\hat{s}_\downarrow) \mathcal{G}(\hat{s}_\uparrow, \hat{s}_\downarrow) \right\}, \quad (27)$$

with the abbreviation

$$\int_0^{2t} d\hat{s}_\sigma \equiv \int_0^{2t} d\hat{s}_{2\tilde{n}_\sigma}^\sigma \int_0^{\hat{s}_{2\tilde{n}_\sigma}^\sigma} d\hat{s}_{2\tilde{n}_\sigma-1}^\sigma \dots \int_0^{\hat{s}_2^\sigma} d\hat{s}_1^\sigma \quad (28)$$

and the restriction that for $\sigma = \uparrow$ no integration is performed over the fixed measurement time $\hat{s}_{n_\sigma+1} = s_{n_\sigma+1} \equiv t$. The influence of the contacts is now summarized in

$$\mathcal{L}_\downarrow(\hat{s}_\downarrow) = (-1)^{n_\downarrow} i^{\tilde{n}_\downarrow} \det(\mathcal{S}(\vec{s}_\downarrow)), \\ \mathcal{L}_\uparrow^{(\alpha)}(\hat{s}_\uparrow) = i^{\tilde{n}_\uparrow} \det(\mathcal{S}^{(\alpha)}(\vec{s}_\uparrow)), \quad (29)$$

where

$$\mathcal{S}_{ij}(\vec{s}_\downarrow) = \begin{cases} \hat{\Sigma}^{-+}(s_{2j-1}^\downarrow, s_{2i}^\downarrow) & \text{for } i \leq j, \\ \hat{\Sigma}^{+-}(s_{2j-1}^\downarrow, s_{2i}^\downarrow) & \text{for } i > j, \end{cases} \quad (30)$$

and $\mathcal{S}_{ij}^{(\alpha)}(\vec{s}_\uparrow)$ is obtained from $\mathcal{S}_{ij}(\vec{s}_\uparrow)$ by replacing $\hat{\Sigma}^{kl}$ by $\hat{\Sigma}_\alpha^{kl}$ whenever one of the time arguments is equal to the measurement time $s_{n_\uparrow+1}^\uparrow = t$. Here, $\hat{\Sigma}_\alpha^{-+}$ ($\hat{\Sigma}_\alpha^{+-}$) denotes the dot's lesser (greater) self energy with respect to the α contact, and $\hat{\Sigma}^{kl} = \sum_\alpha \hat{\Sigma}_\alpha^{kl}$.⁶⁸ Using the bandwidth profile (23) we obtain

$$\hat{\Sigma}_\alpha^{-k,k}(s, s') = -\frac{g(s)g(s')\Gamma_\alpha}{2\beta \sinh(\pi(s-s')/\beta)} \left[k \frac{e^{k\beta\mu_\alpha}}{1 - e^{-2\beta\epsilon_c}} \left(\frac{e^{-i\epsilon_c(s-s')}}{e^{k\beta\mu_\alpha} - e^{k\beta\epsilon_c}} - \frac{e^{i\epsilon_c(s-s')}}{e^{k\beta\mu_\alpha} - e^{-k\beta\epsilon_c}} \right) \right. \\ \left. + \frac{e^{-i\mu_\alpha(s-s')}}{(e^{-\beta\epsilon_c} - e^{-\beta\mu_\alpha})(e^{-\beta\epsilon_c} - e^{\beta\mu_\alpha})} \right], \quad (31)$$

with $k = \pm$. Finally, the contribution from the dot operators to Eq. (27) is given by

$$\mathcal{G}(\hat{s}_\uparrow, \hat{s}_\downarrow) = \mathcal{D}(\vec{s}_\uparrow) \mathcal{D}(\vec{s}_\downarrow) \mathcal{U}(\vec{s}_\uparrow, \vec{s}_\downarrow, n_\downarrow), \quad (32)$$

with

$$\mathcal{D}(\vec{s}_\sigma) = e^{i\epsilon_D(s_1^\sigma - s_2^\sigma + s_3^\sigma - \dots)} e^{i\epsilon_D(s_{2\tilde{n}_\sigma}^\sigma - s_{2\tilde{n}_\sigma-1}^\sigma + s_{2\tilde{n}_\sigma-2}^\sigma - \dots)} \quad (33)$$

and

$$\mathcal{U}(\hat{s}_\uparrow, \hat{s}_\downarrow) = \exp \left\{ iU [\tau_{\text{double}}^{(f)}(\vec{s}_\uparrow, \vec{s}_\downarrow) - \tau_{\text{double}}^{(b)}(\vec{s}_\uparrow, \vec{s}_\downarrow)] \right\}. \quad (34)$$

Here $\tau_{\text{double}}^{(f/b)}$ denotes the time during which the dot is doubly occupied on the forward/backward contour.

In order to calculate the conductance $g_M(t)$ as a function of μ_M in the limit of vanishing tunneling coupling to the third contact ($\Gamma_M \rightarrow 0$), we first note that

$$\frac{d}{d\mu_M} \hat{\Sigma}^{-k,k}(s) = \frac{d}{d\mu_M} \hat{\Sigma}_M^{-k,k}(s) \propto \Gamma_M. \quad (35)$$

Next we proceed by collecting all contributions to

$$\frac{d}{d\mu_M} \det(\mathcal{S}) \det(\mathcal{S}^{(M)}) \quad (36)$$

in lowest (linear) order in Γ_M while neglecting all higher-order terms. In the limit $\Gamma_M \rightarrow 0$ we find that

$$\frac{d}{d\mu_M} \det(\mathcal{S}) \propto \Gamma_M, \quad (37)$$

$$\det(\mathcal{S}^{(M)}) \propto \Gamma_M, \quad (38)$$

$$\frac{d}{d\mu_M} \det(\mathcal{S}^{(M)}) = \det(\tilde{\mathcal{S}}) + \mathcal{O}(\Gamma_M^2), \quad (39)$$

with

$$\tilde{\mathcal{S}}_{ij}(\vec{s}_\uparrow) = \begin{cases} \frac{d}{d\mu_M} \hat{\Sigma}_M^{-+}(s_{2k-1}^\uparrow, t) & \text{for } j = n_\uparrow + 1, k \leq j, \\ \frac{d}{d\mu_M} \hat{\Sigma}_M^{+-}(s_{2k-1}^\uparrow, t) & \text{for } j = n_\uparrow + 1, k > j, \\ \hat{\Sigma}^{-+}(s_{2k-1}^\uparrow, s_{2j}^\uparrow) & \text{for } j \neq n_\uparrow + 1, j \geq k, \\ \hat{\Sigma}^{+-}(s_{2k-1}^\uparrow, s_{2j}^\uparrow) & \text{for } j \neq n_\uparrow + 1, j > k. \end{cases} \quad (40)$$

Since $[d \det(\mathcal{S})/d\mu_M] \det(\mathcal{S}^{(M)})$ is quadratic in Γ_M while $\det(\mathcal{S})[d \det(\mathcal{S}^{(M)})/d\mu_M]$ is linear, we arrive at

$$\frac{d}{d\mu_M} \det(\mathcal{S}^{(M)}) \det(\mathcal{S}) = \det(\tilde{\mathcal{S}}) \det(\mathcal{S}) + \mathcal{O}(\Gamma_M^2), \quad (41)$$

and the third-terminal conductance is found to read

$$\lim_{\Gamma_M \rightarrow 0} \frac{g_M(t)}{\Gamma_M} = -2e \sum_{\substack{\tilde{n}_\uparrow=1 \\ \tilde{n}_\downarrow=0}}^{\infty} (-1)^{\tilde{n}_\uparrow+\tilde{n}_\downarrow} \int_0^{2t} d\hat{s}_\uparrow \int_0^{2t} d\hat{s}_\downarrow (-1)^{n_\downarrow} \\ \times \text{Re} \left\{ \frac{\det(\tilde{\mathcal{S}}(\vec{s}_\uparrow))}{\Gamma_M} \det(\mathcal{S}(\vec{s}_\downarrow)) \mathcal{G}(\hat{s}_\uparrow, \hat{s}_\downarrow) \right\}. \quad (42)$$

Note that in the zero temperature limit,

$$\frac{d}{d\mu_M} \hat{\Sigma}_\alpha^{-k,k}(s, s') \stackrel{T=0}{=} i \frac{g(s)g(s')\Gamma_\alpha}{2\pi} e^{-i\mu_\alpha(s-s')} \quad (43)$$

so that $g_M(t)$ becomes independent of the bandwidth of the third contact.

A crucial point in the simulation is the attainment of the steady state, in which the transport current stops to be time-dependent. The further the system is propagated in time, starting from the initial time $t = 0$ when the tunneling is switched on, the closer the measured current is to the actual steady state value. Unfortunately, this time evolution requires a rapidly increasing computation

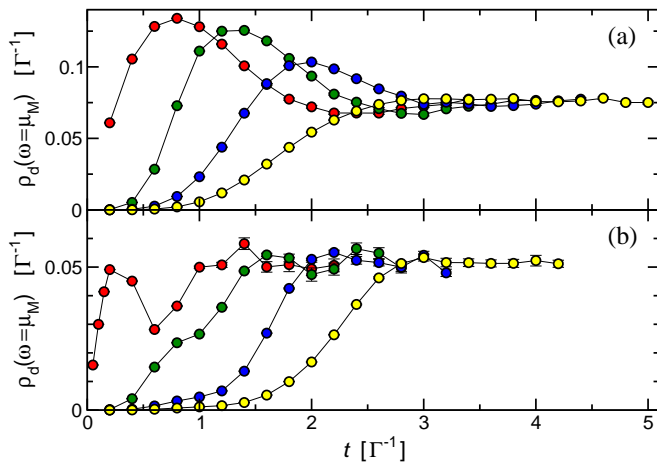


FIG. 4: Spectral function $\rho_d(\omega = \mu_M)$ at zero temperature and $V = 2\Gamma$ for (a) $U = 0 = \epsilon_D$, $\mu_M = 2\Gamma$ and (b) $U = 4\Gamma = -\epsilon_D/2$, $\mu_M = 4\Gamma$. Both panels show data corresponding to four different switching times $\tau_{sw} = 0, \Gamma^{-1}, 2\Gamma^{-1}$, and $3\Gamma^{-1}$ (red, green, blue, and yellow, respectively). The lines are guides to the eye only.

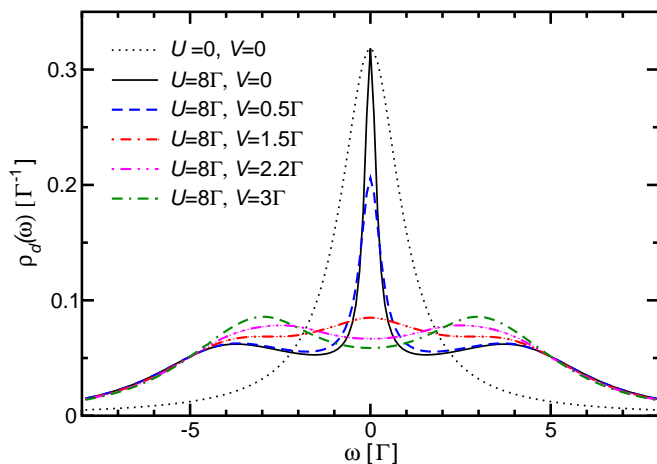


FIG. 5: Zero temperature dot spectral function for different interaction strengths and bias voltages. The curves shown are deduced from the analytical result (15) of the perturbative calculation.

time. Still it has been shown in recent works^{37,41,52} that in many cases the steady state is indeed accessible with moderate numerical effort. As shown in Fig. 4, in our case the steady state of $g_M(t)$ is typically preceded by strongly non-monotonic dynamics. These elongate the transient regime and increase the timescale on which the steady-state regime is reached. However, this timescale can be vastly reduced by adopting a smooth switching of the tunneling coupling according to Eq. (21), thereby extending significantly the parameter regime for which the steady state can be reached.⁵²

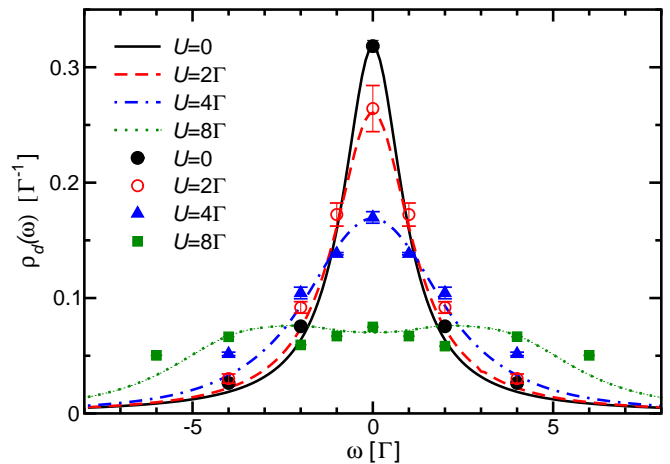


FIG. 6: Zero temperature dot spectral function for different interaction strengths and fixed bias voltage $V/\Gamma = 2$. The points are numerical diagMC data and curves are the analytical results in the second order in U perturbation theory. The slight mismatch of the $U = 0$ data points and the analytical curve is due to finite bandwidth used in the numerical simulations (i. e. a bandwidth of $2\epsilon_c/\Gamma = 12$ for $U/\Gamma \leq 4$ and $2\epsilon_c/\Gamma = 20$ for $U/\Gamma = 8$).

IV. RESULTS AND DISCUSSION

We would like to summarize the results based on the second order self-energy first, see Fig. 5. This approximation is known to *qualitatively* reflect all features one expects in the low energy sector. At vanishing voltage one obtains the typical trident-shaped curve. The central peak in this particular case can be regarded as the precursor of the in reality much sharper Kondo (Abrikosov-Suhl) resonance² having a width (in equilibrium) which can be estimated as³

$$T_K \sim \frac{\sqrt{2U\Gamma}}{\pi} e^{-\pi U/(8\Gamma)}. \quad (44)$$

This formula gives $T_K \sim 0.055\Gamma$ for $U/\Gamma = 8$, which is much smaller than the actual width of the resonance $\tilde{T}_K \sim \Gamma$. The two much wider peaks (shoulders), which are located at $\omega \approx \pm U/2$ are the Hubbard sidebands. Keeping $T = 0$ and increasing the bias voltage does not appear to produce any noticeable qualitative change until V hits the threshold of $\approx \Gamma$, beyond which the ‘Kondo’-peak rapidly deteriorates and completely disappears for $V > \Gamma$. Interestingly, a very similar destruction of the central peak can be observed in equilibrium $V = 0$ at finite temperature $T > \tilde{T}_K$. We thus conjecture that the effect of the finite voltage might be captured by an effective temperature $T_{\text{eff}} \sim V$.

Further insight is gained through the numerical diagMC simulations for the spectral function at finite voltage and U . The numerical data, shown in Fig. 6, turn out to be in an excellent agreement with the analytical results using the second order self-energy up to the

interaction strength $U/\Gamma = 2$. The matching of the perturbative curve and numerical data is still agreeable even at $U/\Gamma = 4$. At $U/\Gamma = 8$ one recognizes the very weak remnants of the Kondo peak at $\omega = 0$ while the rest of the curve has a similar qualitative behavior as the perturbative result and the same order of magnitude. This suggests that the complicated collective multi-particle effects contained in the full self-energy (i.e. exact in U) only have a weak effect and that the main information is already accounted for by the lowest order self-energy discussed in Sec. II. This observation is again compatible with the existence of an effective temperature. We would like to emphasize that T_{eff} is different from the decoherence rate discussed, e. g., in Refs. [15,25–27,30] as this is not defined in the perturbative regime.

In the voltage regimes considered, diagMC does not produce any evidence for the Kondo peak splitting. The relatively high applied voltage $V \sim T_{\text{eff}} \gg T_K$ appears to induce a widening of the Kondo resonance, which renders the observation of the peak splitting impossible. For the diagMC approach outlined in Sec. III, smaller voltages lead to an increase of the timescale over which time-dependent transport properties have to be monitored until a stable stationary regime can be identified. This significantly increases the computational effort necessary to extract the steady-state values. Therefore, in the system under consideration and the numerical scheme and equipment used, it is not yet possible to give a final answer to the question of the Kondo peak doubling with satisfactory precision.

A very interesting issue is the characteristic time scale necessary for the Kondo effect to fully develop. In the

context of a sudden gate voltage quench this problem was discussed in Ref. [65]. On general grounds one would expect that the Kondo peak develops on the time scale $\sim 1/T_K$, as T_K is the only energy scale available in the system in equilibrium. We observe, however, that even in the case of large $U = 8\Gamma$ the steady state of the spectral density at the position of the Kondo peak $\omega = 0$ does not take a longer time to establish than for the energies outside of the Kondo peak. The only exception are the Hubbard subbands $\omega \approx \pm U/2$, where the time development appears to be very slow.

To summarize, we present numerical and analytical results for the impurity spectral function of the symmetric Anderson model in nonequilibrium at zero temperature. We find an excellent agreement of the numerically exact diagMC data with the perturbative expansion of the lowest order in interaction. For larger U we observe a small peak due to the Kondo resonance, which does not show a splitting due to finite applied voltage.

Acknowledgments

The authors are supported by the Kompetenznetz “Funktionelle Nanostrukturen III” of the Baden-Württemberg Stiftung (Germany) and by the DFG under grant No. KO 2235/3. L.M. acknowledges the use of the computing resources provided by the Black Forest Grid Initiative. The authors would like to thank A. O. Gogolin and H. Grabert for many interesting discussions.

-
- ¹ P. W. Anderson, Phys. Rev. **124**, 41 (1961).
 - ² A. C. Hewson, *The Kondo Problem to Heavy Fermions* (Cambridge University Press, Cambridge, 1997).
 - ³ A. M. Tsvelick and P. B. Wiegmann, Adv. Physics (New York) **32**, 453 (1983).
 - ⁴ D. Goldhaber-Gordon, H. Shtrikman, D. Mahalu, D. Abusch-Magder, U. Meirav, and M. A. Kastner, Nature **391**, 156 (1998).
 - ⁵ S. M. Cronenwett, T. H. Oosterkamp, and L. P. Kouwenhoven, Science **281**, 540 (1998).
 - ⁶ J. Schmid, J. Weis, K. Eberl, and K. von Klitzing, Physica B **256-258**, 182 (1998).
 - ⁷ S. Hershfield, J. H. Davies, and J. W. Wilkins, Phys. Rev. B **46**, 7046 (1992).
 - ⁸ Y. Meir, N. S. Wingreen, and P. A. Lee, Phys. Rev. Lett. **70**, 2601 (1993).
 - ⁹ K. Haule, S. Kirchner, J. Kroha, and P. Wölfle, Phys. Rev. B **64**, 155111 (2001).
 - ¹⁰ A. Oguri, J. Phys. Soc. Jpn. **71**, 2969 (2002).
 - ¹¹ R. M. Konik, H. Saleur, and A. Ludwig, Phys. Rev. B **66**, 125304 (2002).
 - ¹² M. H. Hettler, J. Kroha, and S. Hershfield, Phys. Rev. B **58**, 5649 (1998).
 - ¹³ A. Komnik and A. O. Gogolin, Phys. Rev. B **69**, 153102 (2004).
 - ¹⁴ Z. Ratiani and A. Mitra, Phys. Rev. B **79**, 245111 (pages 22) (2009), URL <http://link.aps.org/abstract/PRB/v79/e245111>.
 - ¹⁵ H. Schoeller, Eur. Phys. J.-Spec. Top. **168**, 179 (2009).
 - ¹⁶ T. Korb, F. Reininghaus, H. Schoeller, and J. König, Phys. Rev. B **76**, 165316 (pages 15) (2007), URL <http://link.aps.org/abstract/PRB/v76/e165316>.
 - ¹⁷ T. A. Costi and A. C. Hewson, J. Phys.: Condens. Matter **5**, L361 (1993), URL <http://stacks.iop.org/0953-8984/5/L361>.
 - ¹⁸ F. B. Anders, Phys. Rev. Lett. **101**, 066804 (pages 4) (2008), URL <http://link.aps.org/abstract/PRL/v101/e066804>.
 - ¹⁹ S. Kirino, T. Fujii, J. Zhao, and K. Ueda, J. Phys. Soc. Jpn. **77**, 084704 (2008), URL <http://jpsj.ipap.jp/link?JPSJ/77/084704/>.
 - ²⁰ F. Heidrich-Meisner, A. E. Feiguin, and E. Dagotto, Phys. Rev. B **79**, 235336 (pages 6) (2009), URL <http://link.aps.org/abstract/PRB/v79/e235336>.
 - ²¹ J. Rincon, A. A. Aligia, and K. Hallberg, Phys. Rev. B **79**, 121301 (pages 4) (2009), URL <http://link.aps.org/abstract/PRB/v79/e121301>.
 - ²² R. Gezzi, T. Pruschke, and V. Meden, Phys.

- Rev. B **75**, 045324 (pages 14) (2007), URL <http://link.aps.org/abstract/PRB/v75/e045324>.
- ²³ A. Schiller and S. Hershfield, Phys. Rev. B **58**, 14978 (1998).
- ²⁴ P. Coleman, C. Hooley, and O. Parcollet, Phys. Rev. Lett. **86**, 4088 (2001).
- ²⁵ A. Rosch, J. Kroha, and P. Wölfle, Phys. Rev. Lett. **87**, 156802 (2001).
- ²⁶ S. Kehrein, Phys. Rev. Lett. **95**, 056602 (2005).
- ²⁷ M. Pletyukhov, D. Schuricht, and H. Schoeller, Phys. Rev. Lett. **104**, 106801 (2010).
- ²⁸ M. Pustilnik and L. Glazman, J. Phys.: Condens. Matter **16**, R513 (2004), URL <http://stacks.iop.org/0953-8984/16/i=16/a=R01>.
- ²⁹ N. S. Wingreen and Y. Meir, Phys. Rev. B **49**, 11040 (1994).
- ³⁰ A. Kaminski, Y. V. Nazarov, and L. I. Glazman, Phys. Rev. B **62**, 8154 (2000).
- ³¹ E. Lebanon and A. Schiller, Phys. Rev. B **65**, 035308 (2001).
- ³² Q.-F. Sun and H. Guo, Phys. Rev. B **64**, 153306 (2001).
- ³³ S. De Franceschi, R. Hanson, W. G. van der Wiel, J. M. Elzerman, J. J. Wijkema, T. Fujisawa, S. Tarucha, and L. P. Kouwenhoven, Phys. Rev. Lett. **89**, 156801 (2002).
- ³⁴ R. Leturcq, L. Schmid, K. Ensslin, Y. Meir, D. C. Driscoll, and A. C. Gossard, Phys. Rev. Lett. **95**, 126603 (2005).
- ³⁵ N. Shah and A. Rosch, Phys. Rev. B **73**, 081309 (pages 4) (2006), URL <http://link.aps.org/abstract/PRB/v73/e081309>.
- ³⁶ T. L. Schmidt, A. Komnik, and A. O. Gogolin, Phys. Rev. Lett. **98**, 056603 (2007).
- ³⁷ L. Mühlbacher and E. Rabani, Phys. Rev. Lett. **100**, 176403 (pages 4) (2008), URL <http://link.aps.org/abstract/PRL/v100/e176403>.
- ³⁸ T. L. Schmidt, P. Werner, L. Mühlbacher, and A. Komnik, Phys. Rev. B **78**, 235110 (pages 10) (2008), URL <http://link.aps.org/abstract/PRB/v78/e235110>.
- ³⁹ P. Werner, T. Oka, and A. J. Millis, Phys. Rev. B **79**, 035320 (2009).
- ⁴⁰ M. Schiró and M. Fabrizio, Phys. Rev. B **79**, 153302 (2009).
- ⁴¹ P. Werner, T. Oka, M. Eckstein, and A. J. Millis, Phys. Rev. B **81**, 035108 (2010).
- ⁴² N. Andrei, K. Furuya, and J. H. Lowenstein, Rev. Mod. Phys. **55**, 331 (1983).
- ⁴³ Y. Meir and N. S. Wingreen, Phys. Rev. Lett. **68**, 2512 (1992).
- ⁴⁴ K. Yamada, Prog. Theor. Phys. **54**, 316 (1975).
- ⁴⁵ K. Yamada, Prog. Theor. Phys. **53**, 970 (1975).
- ⁴⁶ K. Yosida and K. Yamada, Prog. Theor. Phys. **53**, 1286 (1975).
- ⁴⁷ K. Yosida and K. Yamada, Prog. Theor. Phys. Supp. **46**, 244 (1970).
- ⁴⁸ B. Horvatić and V. Zlatić, Phys. stat. sol. **99**, 251 (1980).
- ⁴⁹ V. Zlatić and B. Horvatić, Phys. Rev. B **28**, 6904 (1983).
- ⁵⁰ M. Hamasaki, Condensed Matter Physics **10**, 235 (2006).
- ⁵¹ S. Weiss, J. Eckel, M. Thorwart, and R. Egger, Phys. Rev. B **77**, 195316 (pages 12) (2008), URL <http://link.aps.org/abstract/PRB/v77/e195316>.
- ⁵² L. Mühlbacher, unpublished (2010).
- ⁵³ T. Fujii and K. Ueda, Phys. Rev. B **68**, 155310 (2003).
- ⁵⁴ C. Caroli, R. Combescot, P. Nozieres, and D. Saint-James, J. Phys. C **4**, 916 (1971).
- ⁵⁵ A. O. Gogolin and A. Komnik, Phys. Rev. B **73**, 195301 (2006).
- ⁵⁶ R. Egger and A. O. Gogolin, Phys. Rev. B **77**, 113405 (2008).
- ⁵⁷ E. M. Lifshits and L. P. Pitaevskii, *Physical Kinetics* (Pergamon Press, Oxford, 1981).
- ⁵⁸ A. Komnik, Phys. Rev. B **79**, 245102 (pages 5) (2009), URL <http://link.aps.org/abstract/PRB/v79/e245102>.
- ⁵⁹ M. Eckstein, M. Kollar, and P. Werner, Phys. Rev. B **81**, 115131 (2010).
- ⁶⁰ Z. Ratiani and A. Mitra, Phys. Rev. B **81**, 125110 (2010).
- ⁶¹ M. Heyl and S. Kehrein, J. Phys.: Condens. Matter **22**, 345604 (2010), URL <http://stacks.iop.org/0953-8984/22/i=34/a=345604>.
- ⁶² F. B. Anders and A. Schiller, Phys. Rev. Lett. **95**, 196801 (2005).
- ⁶³ C. Karrasch, S. Andergassen, M. Pletyukhov, D. Schuricht, L. Borda, V. Meden, and H. Schoeller, EPL **90**, 30003 (2010), URL <http://stacks.iop.org/0295-5075/90/i=3/a=30003>.
- ⁶⁴ A.-P. Jauho, N. S. Wingreen, and Y. Meir, Phys. Rev. B **50**, 5528 (1994).
- ⁶⁵ P. Nordlander, M. Pustilnik, Y. Meir, N. S. Wingreen, and D. C. Langreth, Phys. Rev. Lett. **83**, 808 (1999).
- ⁶⁶ A generalization to an asymmetrically coupled system is straightforward. To simplify notation we concentrate on the symmetric system.
- ⁶⁷ The retarded polarization loop $\Pi^R(\omega)$ is directly related to the dynamical spin/charge susceptibilities.^{46,49}
- ⁶⁸ Note that the selfenergy $\tilde{\Sigma}$ of Sec. III is defined with respect to the coupling to the leads Γ while the selfenergy Σ of Sec. II is defined with respect to the interaction strength U .